Nuclear Engineering and Technology 54 (2022) 30–35

Contents lists available at ScienceDirect

Nuclear Engineering and Technology

journal homepage: www.elsevier.com/locate/net

Original article

On-line measurement and simulation of the in-core gamma energy deposition in the McMaster nuclear reactor

Mohammed Alqahtani [a, b]

[a] McMaster University, Department of Engineering Physics, Hamilton, Ontario, Canada
[b] Nuclear Science Research Institute (NSRI), KACST, Riyadh, Saudi Arabia

ARTICLE INFO

Article history:
Received 1 July 2021
Received in revised form
26 July 2021
Accepted 26 July 2021
Available online 28 July 2021

Keywords:
Irradiation site
Gamma heating
Gamma thermometer
Fuel assembly

ABSTRACT

In a nuclear reactor, gamma radiation is the dominant energy deposition in non-fuel regions. Heat is generated upon gamma deposition and consequently affects the mechanical and thermal structure of the material. Therefore, the safety of samples should be carefully considered so that their integrity and quality can be retained. To evaluate relevant parameters, an in-core gamma thermometer (GT) was used to measure gamma heating (GH) throughout the operation of the McMaster nuclear reactor (MNR) at four irradiation sites. Additionally, a Monte Carlo reactor physics code (Serpent-2) was utilized to model the MNR with the GT located in the same irradiation sites used in the measurement to verify its predictions against measured GH. This research aids in the development of modeling, calculation, and prediction of the GH utilizing Serpent-2 as well as implementing a new GH measurement at the MNR core. After all uncertainties were quantified for both approaches, comparable GH profiles were observed between the measurements and calculations. In addition, the GH values found in the four sites represent a strong level of radiation based on the distance of the sample from the core. In this study, the maximum and minimum GH values were found at 0.32 ± 0.05 W/g and 0.15 ± 0.02 W/g, respectively, corresponding to 320 Sv/s and 150 Sv/s. These values are crucial to be considered whenever sample is planned to be irradiated inside the MNR core.

1. Introduction

The McMaster nuclear reactor (MNR) is designed to host several experiments and to provide simultaneous irradiation in its core reflector and irradiation sites. The MNR is the world's only supplier of I-125 radioisotope, which is used for male prostate brachytherapy, and one of only a few suppliers of Ho-166, which is utilized in many applications. Most of these isotopes are produced by irradiation in the reactor core, and some of these isotopes are susceptible to damage under high radiation levels (energy) or high temperatures. Gamma heating (GH), or energy deposition, is primarily responsible for temperature rises in the non-fuelled zones of nuclear reactors [1].

An in-core sample irradiation experiment was previously conducted by a group of researchers at the MNR to irradiate a medical isotope device based on Ho-165 and found that massive damage was incurred by Ho-166 microspheres. This study suggested that GH was the primary cause of the damage to the microsphere sample [2]. A lack of GH evaluations is a major limitation for any irradiation application and leads to a lack of optimal irradiation conditions [3]. Accordingly, in 2019–2020, GH measurements and calculations were performed at the MNR for three irradiation sites in 27 GH regions [4]. The results showed that most of the GH values found by the two methods agreed within the level of uncertainty. Additionally, the observed values were sufficient to cause damage. These findings are crucial for evaluating and predicting GH parameters for future irradiation experiments.

However, this previous research has limitations in both representing the decay GH and considering instrument uncertainties. The calculated decay GH in the previous investigation was based on a correction factor implemented in the Monte Carlo Serpent-2 code to approximate the delayed gamma energy deposition as the prompt gamma energy distribution. However, in Ref. [5], the authors studied the accuracy of implementing a correction factor and concluded that in order to more accurately calculate the delayed gamma energy deposition, a delayed gamma source must be produced by solving the Bateman equations [6].

E-mail addresses: Alqahm1@mcmaster.ca, malqahtani@kacst.edu.sa.

https://doi.org/10.1016/j.net.2021.07.040

Therefore, the aim of this work is to (i) calculate the decay GH during reactor operation by solving the Bateman equations, (ii) perform additional GH measurements at the reflector site, and (iii) verify the calculated and measured GH values with for the MNR core, along with three previous GH measurements and calculations (four irradiation sites in total). Measurements were performed by using a differential temperature thermocouple and a gamma thermometer (GT), which is described in detail later in this work.

The most important advantage of the calculation implemented in this work is that it can implement the Bateman equations and track all gamma particles in the MNR Serpent-2 simulation model based on fuel irradiation (burn-up). Additionally, a more thorough consideration of the uncertainties associated with the measurements is included and implementing another in-core GH measurement in the reactor core.

2. Description of the MNR

The MNR is an MTR-type reactor that is fuelled by low-enriched uranium (19.75 %). The core grid consists of 6-by-9 assemblies, including 32 standard fuel assemblies (SFAs), 6 control fuel assemblies (CFAs), 7 graphite reflector assemblies, and 1 beryllium assembly [7,8]. Light water is used as both the moderator and coolant of the MNR. The in-core irradiation sites are situated in a graphite reflector and a beryllium reflector. The irradiation diameters of the beryllium and graphite reflectors are 3.81 and 3.50 cm, respectively. Table 1 provides the general parameters for the MNR, and Fig. 1 illustrates the MNR core configuration.

3. Methods

3.1. Measurement set-up

A small gamma thermometer (GT), manufactured by SCK-CEN in Belgium, was used to perform GH measurements at four irradiation sites [9]. The GT measures GH through a differential temperature thermocouple between hot and cold junctions. The operation of the GT is based on the two dissimilar metals always have a contact potential between them, which varies as the temperature changes. There are two junctions in a circuit; when these two junctions experience different temperatures, then a voltage can be detected and measured. Fig. 2 provides a cross-sectional view of the GT and its dimensions in millimeters.

The GT and the differential thermocouple are made of AISI 304 and AISI 316 L stainless steel material, respectively. The hot junction, which forms the inner GT core, is insulated by argon gas at 1.25 MPa. This inner junction can be primarily heated by gamma radiation and eventually becomes warmer than the cold junction. The outer (cold) junction is continuously cooled by the coolant flow and can be assumed to have a temperature similar to the coolant temperature of the reactor core. The inlet and outlet reactor coolant temperatures were recorded at approximately 30° and 36 °C, respectively.

The GT uses a K-type thermocouple that processes data (voltage) whenever a temperature difference arises between the hot and cold junctions. These signals based on a temperature difference, which creates a voltage, are recorded in data acquisition hardware for obtaining temperature data using thermocouples in LabVIEW at a frequency of 1 Hz.

The instrument rig used to carry the GT was specifically designed and manufactured to accommodate the GT at any irradiation site in the MNR core, i.e., at both graphite and beryllium reflectors. The rig comprises an inner race and an outer body. The outer body is fixed after it is mounted on the graphite/beryllium site, whereas the inner race can by axially placed at any level [11]. Each measurement was performed twice, i.e., top-to-bottom and bottom-to-top, for each irradiation site.

For each axial GH measurement, either bottom-to-top or top-to-bottom, an average of ten GH values was obtained after a period of five-time constants. This approach results in less uncertainty when collecting several data points.

Four irradiation sites (2A, 8B, 8E, and 8F) were selected for measurement. For each site, 9 GH values were obtained, for a total of 36 GH values. The reactor power remained constant during the measurement campaign at 3 MW_{th}. All uncertainties were previously evaluated in Ref. [4]; however, this work also includes the GT uncertainty from the manufacturer, which is ±10 %, as well as that of the resistance temperature detector (RTD), which measures the reactor temperature difference across the MNR core.

3.2. Calculation

i Calculation process

Serpent-2 is a three-dimensional (3D) continuous-energy Monte Carlo particle transport code developed by the VTT Technical Research Center of Finland. Various reactor physics applications can be performed in Serpent-2, including criticality calculations (k_{eff}), neutron and photon flux calculations, fuel burn-up calculations, reactor modeling, and modeling of coupled multi-physics applications.

A photon transport mode was introduced in Serpent version 2.1.24 in 2015 [12]. Several features that employ the photon transport have since been developed, such as a coupled

Table 1
MNR general description and core specifications.

Parameter	Specification
Reactor type	Open-pool MTR
Maximum/nominal power	5/3 MW_{th}
Maximum neutron flux (3 MW_{th})	5.8×10^{13} n/cm^{2}s
Coolant and moderator	Light water
Reflector	Graphite and beryllium
Coolant circulation	Natural circulation or forced downward flow
Fuel type	U_3Si_2–Al dispersion Al-clad plate fuel
Fresh SFA and CFA atom density	1.89×10^{-3} and 1.67×10^{-3} at/b.cm
Enrichment	19.75 %
Control system	5 Ag–In–Cd shim safety rods and 1 stainless steel rod
Plate, fuel meat, and cladding thickness	0.127, 0.051, and 0.038 cm
Core lattice size, x and y	8.1 and 7.709 cm
Core height	60 cm

CFA, control fuel assembly; SFA, standard fuel assembly.

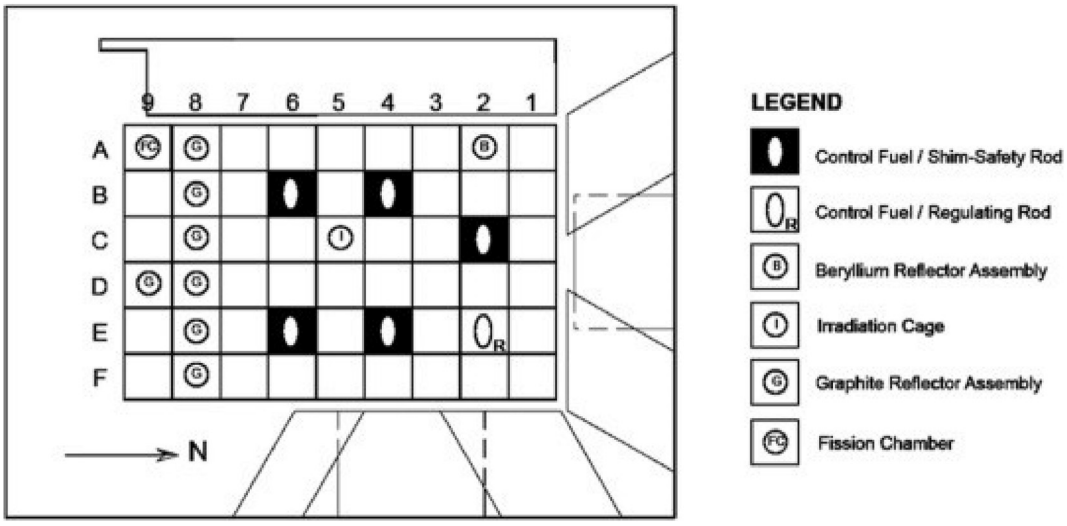

Fig. 1. Top view of the MNR core.

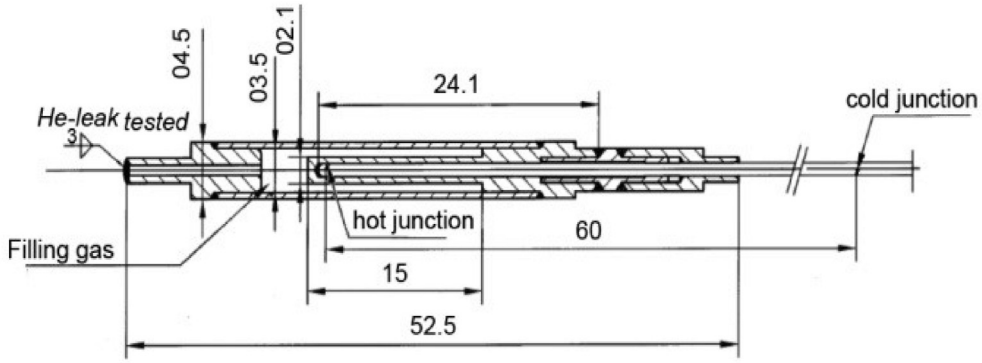

Fig. 2. Schematic view of the GT built by SCK-CEN and its dimensions in millimeters [10].

neutron–photon transport mode [13] and a radioactive decay source mode [14]. In this work, the recent development of photon physics in Serpent-2 was utilized to estimate the energy deposition carried out by particles to non-fuel regions [15].

In the energy deposition mode, calculations are performed whenever a photon or neutron interaction occurs. For example, photon energy deposition occurs via the photoelectric effect, Compton scattering, and pair production. The nuclear heating, or neutron/photon heating, calculation in Serpent-2 can be expressed as

$$\sum_i \sum_j \rho_i k_{ij}(E)\Phi(E) \tag{1}$$

where ρ_i is the atomic density of nuclide i, k_{ij}(E) is the KERMA coefficient for nuclide i and reaction j at incident energy E, and Φ(E) is the scalar neutron/photon flux. KERMA coefficients were obtained from the NJOY nuclear data processing code [16], which is necessary for heat deposition.

There are four modes (0–3) in Serpent-2 for calculating the energy deposition. Mode 3 is the most accurate, where coupled neutron/photon transport is applied to track both neutron and photon particles until they disappear. In this mode, the fission site energy deposition, which is calculated from ENDF MF1 MT458 data [17], is given by

$$E_{fiss,i} = EFR + EB \tag{2}$$

where EFR denotes the kinetic energy of the fission products and EB is the delayed beta energy. These two energy components, EFR and EB, are deposited at the fission site (origin), while photons and neutrons dissipate their energy through the medium in the core.

In reference [4], the delayed gamma energy deposition was calculated by approximating the distribution as the prompt gamma energy distribution. However, in this work, the delayed gamma energy deposition was more accurately calculated by solving the Bateman equations to produce a delayed gamma source. The calculation of the Bateman equations can be read from a binary file, which contains all fission products and activated materials in the reactor. This calculation is performed in the secondary simulation following a prompt calculation. The disadvantage of this calculation is that is requires a long computational time to first track the prompt gamma from fission and (n,g) reaction, then another calculation for gammas from activated isotopes or fission products.

ii MNR Serpent-2 model

The MNR Serpent-2 model includes the reactor core configuration that houses the MTR fuel, the graphite reflector, the beryllium assembly, and the surrounding beams. The MNR fuel composition was extracted based on operational data history for the reactor core. The extraction of fuel composition from the

measurement-base estimate followed the procedure provided in Ref. [18]. The nuclear data library used in this model is ENDF/B-VII.1 [19].

The GT instrument was modeled with the same materials that were provided, as described in Section 3.1. All statistical uncertainties were maintained below 1.7 % in all GH calculations, with 3000 active histories and 90,000 particles per history for a total of 2.7×10^8 particles. The calculational time for this simulation was 13.2 h with 20 OMP parallel threads. Whereas the decay number pf particles used are 8×10^8 particles. Due to the computational time, a simple approximation was implemented in the GT calculation model by assuming that the energy deposition occurred between the hot and cold junctions. Fig. 3 illustrates the MNR Serpent-2 model used in this research.

4. Results and analysis

4.1. Uncertainty quantification

A series of measurements and simulations was conducted to evaluate parameters that can influence the calculated/measured GH quantities. The combined uncertainty was studied and reported in Ref. [4] at approximately 9 % with two standard deviations (95 % confidence interval). However, this uncertainty does not include two major components: (i) the GT instrument uncertainty from the calibration factor specified by the manufacturer, which is equal to 10 %, and (ii) the uncertainty from to the RTDs, which are located above and below the MNR core to continuously measure temperatures for core power monitor in the control room.

The major GH sources during reactor operation are the prompt GH, which includes both fission gamma and (n,g) reactions, and the decay of short half-life fission fragments. Both sources vary based on local power variations. Therefore, the GH source is dependent on the reactor core power, which was maintained at 3 MW_{th} during the measurement. However, the MNR core measures the power by means of a temperature difference between the core inlet and outlet. The MNR uses a class-B-type RTD to measure the temperature and consequently the core power. The core power can be calculated from

$$P = mC_p(T_{out} - T_{in}) \tag{3}$$

where m is the mass flow rate, C_p is the specific heat capacity, T_{in} is the inlet temperature, and T_{out} is the outlet temperature measured downstream of the core by the RTD. The RTD has a tolerance bias based on the environment temperature [20]. Fig. 4 illustrates the RTD tolerance as a function of temperature.

The inlet and outlet temperatures in the MNR core are approximately 30 °C and 35.5 °C, respectively. As shown in Fig. 4, the inlet and outlet biases are 0.45 °C and 0.48 °C, respectively. These biases seem low; however, deviations can arise from the actual reading depending on the temperature difference and flow rate, as shown in Equation (3). In the MNR core, the temperature difference between the inlet and outlet is approximately 5.5 °C; therefore, the reactor power bias can be estimated within approximately 8 %.

Here, we combine the uncertainties from the GT and RTD instruments with the uncertainty reported in Ref. [4] and apply the final combined uncertainty as described in Ref. [21] using Equation (4). The final combined uncertainty was obtained at approximately 17 % with two standard deviations. We assumed that the uncertainties of these instruments have a coverage factor of 2. This assumption seems conservative as the instruments both have type-B uncertainties.

$$u_c^2(y) = \sum_{i=1}^{n} u_i^2(y) \tag{4}$$

4.2. GH measurement and verification of Serpent-2 code calculations

The GH results and statistics-related uncertainties demonstrated in the previous section are considered for all measured GH values here. In Fig. 5, four axial GH profiles from four different irradiation sites are displayed based on the GT and Serpent-2 calculations. As expected, among the considered irradiation sites, the beryllium assembly (2A) shows the highest GH due to the fuel assemblies surrounding the GT. Meanwhile, the GH values of the graphite assembly (8F) have the lowest GH values due to the lower surrounding assemblies' power and absence of any nearby fuel assembly, as shown by the core grid in Fig. 3.

Fig. 5 shows the axial GH for four sites in the MNR core. Here, the four lines for each site represent (i) the calculated prompt GH, (ii) the calculated delay GH, (iii) the calculated total GH (prompt + delay), and (iv) the measured GH by the GT.

For all lines (measured and calculated total GH), the maximum

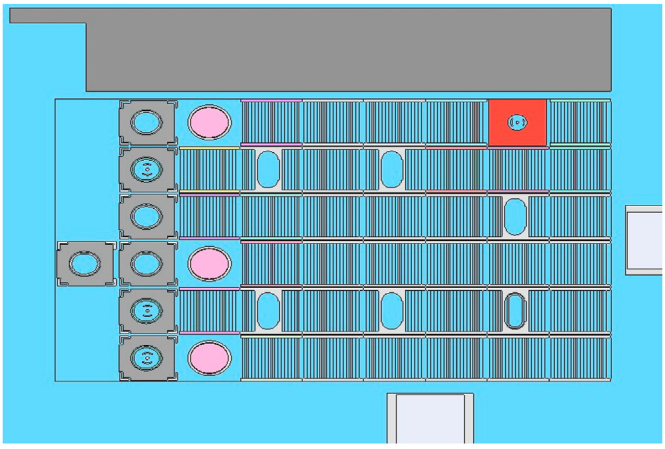

Fig. 3. MNR Serpent-2 model.

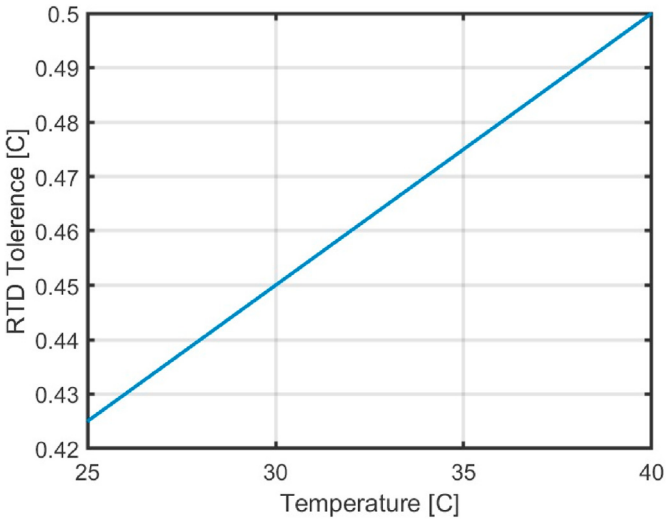

Fig. 4. RTD tolerance vs. environmental temperature.

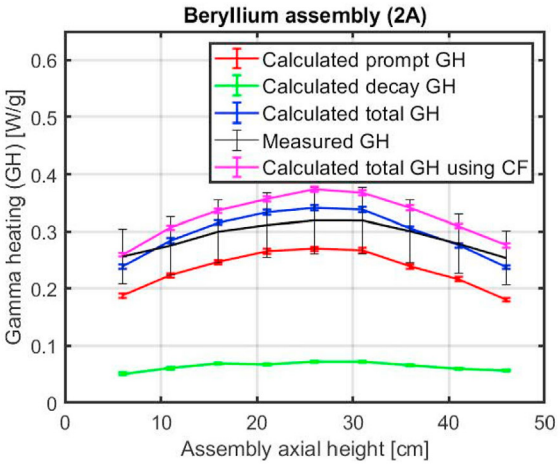

Beryllium assembly (2A).

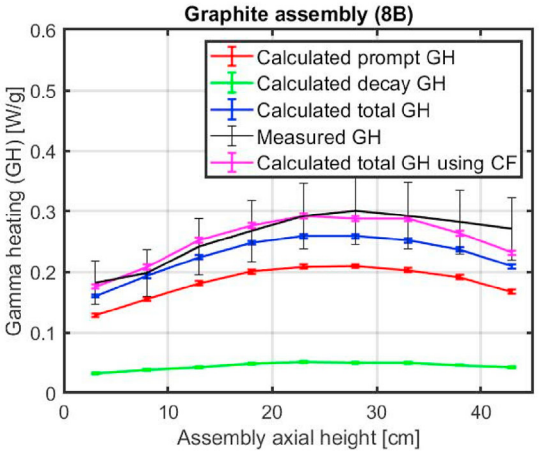

Graphite assembly (8B).

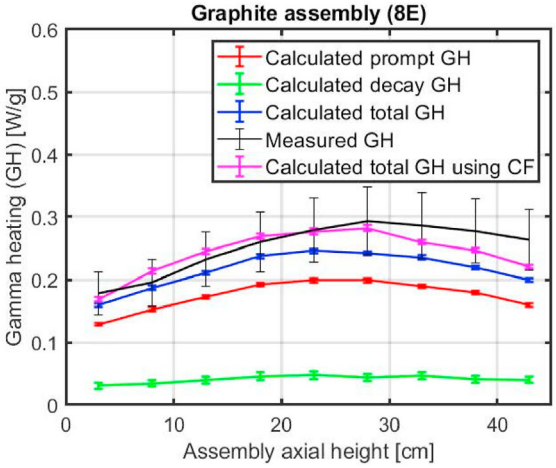

Graphite assembly (8E).

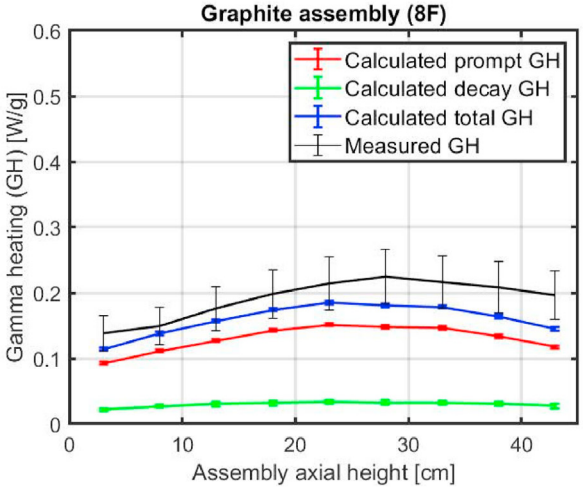

Graphite assembly (8F).

Fig. 5. GH measurement and calculation for four axial irradiation sites with a core power of 3 MW_{th}.

GH value is located at 25–30 cm of the core height. This level is slightly lower than the core center (30 cm), owing to the insertion of control rods from the core top, where the rods were inserted approximately 20 % (6 cm). In addition, in all cases, the measured and calculated GH values are within the uncertainty defined in this paper, except for the highest points in the three graphite assemblies. The notable decrease seen in the upper region of all assemblies is expected due to the CRs worth in Serpent-2 which is slightly higher (9 mk) than the measured MNR CRs worth values. This trend can be confirmed by the GH values in the all irradiation sites, where the upper region showed GH values with more gradual decrease.

Additionally, Fig. 5 shows the calculated delay GH that occurs during the reactor operation. The delay GH contribution to the total GH for all values is 19%–22 %. It is expected that this value is lower than the actual delay GH inside the core owing to limitations in calculating the delay GH emitted from the reactor core structure. The delay GH calculation shown in Fig. 5 considers the dominant delay GH in the core, such as the decay GH from fission fragments and the aluminum structure of the fuel assembly. Notably, the delay GH from the fuel assembly structure contributes a significant portion of the delay GH due to the short half-life of Al-28 when neutrons interact with Al-27, Al27 (n,g)Al-28. The half-life of Al-28 is approximately 2.3 min, with a gamma energy of 1.78 MeV. This trend supports previous evidence regarding the lower delay GH expected in this work, due to the core structure, which predominantly consists of aluminum.

Overall, comparable GH profiles were observed for the four selected sites between the Serpent-2 and measurement results. One limitation in this work is the implementation of the 3D FA calculation, whereas previous calculations were performed via a 3D FA with no consideration of CRs in the core. However, to implement exact modeling, we must consider the effect of the control rod insertion on all FAs, not only on the CFAs. Consequently, another contribution to differences between the measured and calculated GH values arises from this limitation.

The four axial GH values, obtained for 36 regions, are considered to be sufficiently strong to cause damage to some irradiation materials. These values should be considered among the conditions for future irradiation samples.

5. Conclusion

Measured and calculated GH values for four irradiation sites in the MNR core were obtained and compared. The uncertainties of the instruments were included in this work to capture all variables that may cause the GH to shift from its true value. Among 36 calculated GH values, 33 are in good agreement with the measured GH and within the quantified uncertainty. The other three GH values were seen out of the combined uncertainty. It is expected that the CR value causes a higher GH uncertainty/deviation in the upper region, causing these GH values to drift slightly beyond the range of uncertainty. The contribution of the delay GH to the total GH was found to be 19%–22 % of the total GH.

Future research could expand delay GH calculations to account for the MNR core structure. In addition, further investigation is recommended to verify the types of conclusions that can be drawn from this study in examining the thermal behavior of target materials under the GH values presented in this work.

Declaration of competing interest

The authors declare that they have no known competing financial interests or personal relationships that could have appeared to influence the work reported in this paper.

Acknowledgements

The author would like to express gratitude to Dr. Adriaan Buijs and Dr. Simon Day. In addition, he would like to thank the MNR staff for their help during GH measurements. Finally, the author thanks the reactor manager and supervisor, Rob Pasuta and Jay Grigg-Tait, for always being available to answer inquiries regarding the reactor operation.

References

[1] M. Lemaire, C. Vaglio-Gaudard, A. Lyoussi, C. Reynard-Carette, For a better estimation of gamma heating in nuclear material-testing reactors and associated devices: status and work plan from calculation methods to nuclear data, J. Nucl. Sci. Technol. 52 (2015) 1–9, https://doi.org/10.1080/00223131.2015.1009957.

[2] C. Heysel, A. Armstrong, J. Bennett, E. Werger, Z. Naperstkow, R. Pasuta, Canadian nuclear society (CNS), CUSTOMIZED IRRADIATION SITES FOR MEDICAL ISOTOPE PRODUCTION 50 (2018).

[3] Manual for reactor produced radioisotopes, Tech. Rep. IAEATECDOC-1340, International Atomic Energy Agency IAEA, 2003.

[4] M. Alqahtani, A. Buijs, S. Day, Experimental measure and Monte Carlo code simulation of the gamma heating at different irradiation sites in a nuclear research reactor, Nucl. Eng. Des. 364 (2020), 110690, https://doi.org/10.1016/j.nucengdes.2020.110690. URL, https://www.sciencedirect.com/science/article/pii/ S0029549320301849.

[5] Y. Liu, W. Martin, T. Downar, Delayed fission energy effect on LWR normal operation and transients, in: Proceedings of PHYSOR 2018, PHYSOR 2018: Reactor Physics Paving the Way towards More Efficient Systems, Sociedad Nuclear Mexicana., Mexico, 2018.

[6] J.R. Lamarsh, Introduction to Nuclear Reactor Theory, second ed., Addison-Wesley, Reading, MA, 1983.

[7] S. Day, McMaster Nuclear Reactor Specification, IAEA CRP 1496: Innovative Methods for Research Reactors, 2011.

[8] M. Alqahtani, S.E. Days, A. Buijs, OSCAR-4 code system comparison and analysis with a first-order semi-empirical method for core-follow depletion calculation in McMaster nuclear reactor (MNR), CNL Nuclear Review (2019), https://doi.org/10.12943/CNR.2019.00011.

[9] O. Aarestad, In-core instrumentation for LWRs, presented at IAEA meeting on "in-core instrumentation and in-situ measurements in connection with fuel behaviour", held in petten, The Netherlands, October. URL, https://inis.iaea.org/collection/NCLCollectionStore/, 1992. Public/28/018/28018794.pdf.

[10] D. Fourmentel, C. Reynard-Carette, A. Lyoussi, J.F. Villard, J.Y. Malo, M. Carette, J. Brun, P. Guimbal, Y. Zerega, Nuclear Heating Measurements in Material Testing Reactor: A Comparison between a Differential Calorimeter and a Gamma Thermometer, vol. 60, IEEE Transactions on Nuclear Science, 2013, pp. 328–335, 1.

[11] K, Stoll," a Time-dependent Description of In-Core Gamma Heating in the Mcmaster Nuclear Reactor", Ph.D. thesis, McMaster University, 2016.

[12] T. Kaltiaisenaho, Implementing a photon physics model in serpent 2; fotonifysiikkamallin kehittäminen serpent 2-koodiin, G2 pro gradu, diplomityö (2016-06-14), URL, http://urn.fi/URN. NBN:fi:aalto-201606172612.

[13] J. Leppänen, T. Kaltiaisenaho, V. Valtavirta, M. Metsälä, Development of a coupled neutron/photon transport mode in the serpent 2 Monte Carlo code, 2017, international conference on mathematics and computational methods applied to nuclear science and engineering, mamp;C, in: Mamp;C 2017 ; Conference Date: 16-04-2017 through 20-04-2017, 2017.

[14] J. Leppänen, T. Kaltiaisenaho, Expanding the use of serpent 2 to fusion applications: shut-down dose rate calculations, Proceedings of PHYSOR 2016, American Nuclear Society (ANS), United States (2016). ISBN: 978-0-89448-762-2.

[15] R. Tuominen, V. Valtavirta, J. Leppänen, New energy deposition treatment in the serpent 2 Monte Carlo transport code, Ann. Nucl. Energy 129 (2019) 224–232, https://doi.org/10.1016/j.anucene, 2019. 02.003.

[16] R. Macfarlane, D.W. Muir, R.M. Boicourt, A.C. Kahler, J.L. Conlin, The NJOY Nuclear Data Processing System, Tech. Rep. LAUR-17-20093, Los Alamos National Laboratory, 2016.

[17] A. Trkov, M. Herman, D.A. Brown, ENDF-6 formats manual – data formats and procedures for the evaluated nuclear data files ENDF/B-VI, ENDF/B-VII and ENDF/B-VIII., tech. Rep BNL-90365-2009 Rev.2, Brookhaven National Laboratory, 2018. https://www.osti.gov/servlets/purl/1425114.

[18] M. Alqahtani, A. Buijs, S.E. Day, Serpent-2 and OSCAR-4 computational tools compared against McMaster nuclear reactor improved operational data history for U-235 fuel inventory tracking, local power tracking and validation of multiplication factor, Ann. Nucl. Energy 145 (2020) 107590, https://doi.org/10.1016/j.anucene.2020.107590.

[19] M. Chadwick, M. Herman, P. Obložinský, M. Dunn, Y. Danon, A. Kahler, D. Smith, B. Pritychenko, G. Arbanas, R. Arcilla, R. Brewer, D. Brown, R. Capote, A. Carlson, Y. Cho, H. Derrien, K. Guber, G. Hale, S. Hoblit, S. Holloway, T. Johnson, T. Kawano, B. Kiedrowski, H. Kim, S. Kunieda, N. Larson, L. Leal, J. Lestone, R. Little, E. McCutchan, R. MacFarlane, M. MacInnes, C. Mattoon, R. McKnight, S. Mughabghab, G. Nobre, G. Palmiotti, A. Palumbo, M. Pigni, V. Pronyaev, R. Sayer, A. Sonzogni, N. Summers, P. Talou, I. Thompson, A. Trkov, R. Vogt, S. van der Marck, A. Wallner, M. White, D. Wiarda, P. Young, Endf/b-vii.1 nuclear data for science and technology: cross sections, covariances, fission product yields and decay data, Nuclear Data Sheets 112 (12) (2011) 2887–2996, https://doi.org/10.1016/j.nds.2011.11.002. http://www.sciencedirect.com/science/article/pii/S009037521100113X. special Issue on ENDF/B-VII.1 Library, URL.

[20] T.E. Connectivity, Understanding RTDs. https://www.te.com/global-en/industries/ sensor-solutions/insights/understanding-rtds.html, 2020-10-17.

[21] International Bureau of Weights and Measures, Evaluation of measurement data — guide to the expression of uncertainty in measurement, JCGM 2008 (2008).